Mechanical Competence of Bone: A New Parameter to Grade Trabecular Bone Fragility From Tortuosity and Elasticity

Waldir L. Roque*, Katia Arcaro, and Angel Alberich-Bayarri, *Member, IEEE*

***Abstract*—With the elderly population increase, osteoporosis and its consequences have become not just a health issue but also a serious economic burden. The trabecular bone structure plays a very important role for the bone quality and mechanical competence of the scaffold. Currently, it is claimed that the trabecular microarchitecture understanding can improve the fracture risk prediction above 65%. Several parameters seem to be correlated providing structural details of the trabecular bone network. However, the tortuosity of the trabeculae has not yet been systematically taken into account and its contribution has not been fully investigated and understood. In this paper, we discuss the relationship between the trabecular tortuosity, connectivity, volume fraction, and elasticity, and provide a unified parameter to estimate the mechanical competence of the structure. It is shown that the trabecular network tortuosity presents high linear correlation with the other parameters and that the trabeculae tend to get aligned in the direction where the structure is mostly submitted to stress, corresponding to higher stiffness orientation. This new parameter will help to integrate the relevant information of bone microarchitecture quality and assess more directly the real trabecular fragility in osteoporotic patients.**

***Index Terms*—Connectivity, elasticity, mechanical competence, tortuosity, trabecular bone.**

I. Introduction

With the current growth of life expectancy, the raise of osteoporosis has become not just a medical problem, but an economic burden for the private and public health systems. One of the main consequences of the osteoporosis is bone fractures, contributing to the health degradation of elderly patients and morbidity, leading sometimes to obit. This process has a very high cost with estimations for the United States of the order of 25 billions of dollars for the year 2025 [1]. For the Brazilian case, a study has shown that one in each three patients with iliac bone fracture has a diagnostic of osteoporosis and among those, only one in five gets some kind of treatment. During the period of 2003–2005, only the Brazilian private health system had a cost with just hip osteoporotic fracture of the order of 12 million Reais (∼7.5 million U.S. dollars), according to the study published in [2]. Due to the high socioeconomic impact of the disease, new noninvasive and automated techniques [3] are needed for a direct assessment of the real fracture risk in osteoporotic patients.

Osteoporosis is characterized by bone mass loss and degradation of the cancellous bone structure. The cancellous bone is essentially formed by the trabecular bone network and the fatty marrow. The trabecular bone as metabolically more active, it is also more vulnerable and continuously remodels. The gold standard procedure for the osteoporosis diagnosis is the bone mineral density (BMD) evaluation; nevertheless, it is responsible for about 60% of the bone mechanical resistance [4]. On the other hand, recent studies have shown that the trabecular bone microarchitecture can raise this estimate up to 90% [5], [6]. In general, low values of BMD is a warning for fracture risk; however, some patients that present similar values of BMD have serious bone trauma [4], while others do not have. As the BMD is a global measure of the whole bone structure (cortical and cancellous bone), this measure is not able to detect defects and fragilities in the trabecular structure.

With the fast development of medical imaging techniques, going to high spatial resolutions, the extraction of histomorphometrical and geometrical data like the volume fraction, trabecular thickness, connectivity, or elasticity of the trabecular structure has become more feasible. In particular, microcomputer tomography (μCT) has opened up new horizons going down to the nanoscale [7]. In a recent paper [8], it has been shown that there is a positive correlation between the trabecular volume fraction, the connectivity, using the Euler–Poincaré characteristic (EPC), and the Young modulus of elasticity. In [9], a volumetric topological analysis has been proposed and a correlation study between the trabecular bone volume fraction, the average surface width, the surface curve ratio, and the Young modulus was conducted to investigate trabecular bone mechanical properties. All these parameters have shown an important role to establish the mechanical competence of the trabecular bone. In simple terms, the trabecular structure can be seen as a network of columns and beams that provide the mechanical resistance of the structure when subject to stress and strain. However, these columns and beams are not straight, they present a sinuous arrangement

Manuscript received August 21, 2012; revised November 14, 2012; accepted December 10, 2012. Date of publication December 20, 2012; date of current version April 15, 2013. The work of K. Arcaro was supported by the CAPES through a doctoral scholarship. The work of A. Alberich-Bayarri was supported by the Spanish National Research Funding through Project DPI2011-22413. *Asterisk indicates corresponding author.*

*W. L. Roque is with the Federal University of Rio Grande do Sul, Porto Alegre, RS 91509-900, Brazil (e-mail: roque@mat.ufrgs.br).

K. Arcaro is with the Federal University of Rio Grande do Sul, Porto Alegre RS 91509-900, Brazil (e-mail: karcaro@hotmail.com).

A. Alberich-Bayarri is with the Quiron Quantification Group, Quiron Valencia Hospital, Valencia 46010, Spain (e-mail: aalberich.val@quiron.es).

Color versions of one or more of the figures in this paper are available online at http://ieeexplore.ieee.org.

Digital Object Identifier 10.1109/TBME.2012.2234457

and this characteristic is highly relevant to the biomechanical response [10]. Therefore, it has to be taken into account when estimating the mechanical competence of the trabecular bone.

In a porous media, the tortuosity is a measure of the sinuosity of a pore and it has a significant influence for particle transport and wave propagation. There are a few definitions of tortuosity in the literature [11]; nevertheless, the geometric tortuosity is a well-defined mathematical concept for any filamentous object. Cancellous bone can be modeled as a two-phase porous medium (bone and marrow phases). In general, in the study of the trabecular bone, the soft phase is actually reduced to a void phase (cavities). A binary segmentation reduces the porous medium to black and white phases. The trabecular network (white phase) has a sinuous format and so its tortuosity can be estimated and its relationship with other parameters can be investigated. To the authors knowledge, there has been no systematic image-based investigation about the role of the tortuosity of the trabecular bone and its importance to the mechanical competence of the scaffold. More recently, some studies have been conducted using quantitative ultrasound (QUS) to estimate the tortuosity of the cavity network (soft phase) as a structural parameter and its effect on sound propagation in bovine and human cancellous bone [12]–[14].

In this paper, a novel mechanical competence parameter (MCP) is proposed to assess the characterization of trabecular bone fragility from high spatial resolution images. The new parameter takes into account morphometry, connectivity, tortuosity, and elasticity properties of the tissue.

II. Material and Methods

A series of 3-D μCT images of *ex vivo* distal radius trabecular bone was considered from 15 individuals. The samples (side length 12 mm) were harvested with an average distance of 9.75 mm from the endplate of the radius and scanned with a μCT-20 scanner (Scanco Medical, Bruttisellen, Switzerland) considering an isotropic voxel size of 34 μm. The craniocaudal direction was identified with the z-axis of each sample. Further details concerning the sample preparation and image acquisition protocols are described in the previous studies of Laib *et al.* [15]. For this study, 15 individual sets with 239 μCT slices each were considered. The reconstruction matrix dimensions of five samples were $212 \times 212, 237 \times 237, 242 \times 242, 252 \times 252, 257 \times 257$, and all others 268×268 pixels. The 3-D μCT images were filtered with a 3D Gaussian filter. In each case the gray-level histograms of filtered images contained two peaks corresponding to marrow and bone and, thus, images were binarized, using the Otsu's method [16].

The binary matrices of the images were generated using *OsteoImage*, a computer system that is in development by the authors to analyze trabecular bone images. The tortuosity was estimated based on the method described in Section II-A and the geodesic reconstruction (GR) algorithm detailed in the Appendix. The 3-D images presented in this paper were produced with aid of *ImageJ* software (see http://rsbweb.nih.gov/ij/).

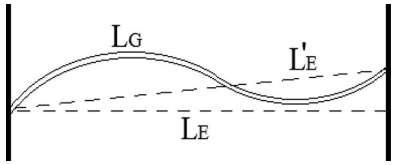

Fig. 1. Geodesic distance L_G and Eucledian distance L'_E between points and L_E between planes.

In the elasticity study, the 3-D trabecular bone structure was meshed using an optimized algorithm [17] implemented in Matlab R2011a (The MathWorks, Inc., Natick, MA), which converts each voxel to an hexahedron element (brick element). Compression stress–strain test in each space direction was numerically simulated by a finite element (FE) linear-elastic-isotropic analysis performed in Ansys v11.0 (Ansys, Inc., Southpointe, PA). The bulk material properties were set to $E_{\mathrm{bulk}} = 10$ GPa (compact bone) [18], [19] and Poisson's coefficient $\nu = 0.3$. A deformation of 1% of the edge length was imposed in all the compression simulations. After application of the homogenization theory [20], apparent Young modulus (E_x, E_y, E_z) results were obtained in each space direction.

Finally, a principal component analysis (PCA) was performed considering the volume fraction, Euler–Poincaré connectivity, tortuosity, and elasticity for the 15 samples, showing that a unique parameter can be defined comprising all of them together. This MCP will help to define the fragility status of the microarchitecture of the trabecular bone for a more reliable assessment of the fracture risk.

A. Trabecular Bone Characteristics

1) Trabecular Network Tortuosities: In a porous media, there are different definitions of tortuosity [11] referring to the sinuosity of a pore. This paper is focused in the geometric tortuosity and extend this concept to the trabeculae. In mathematical terms, the tortuosity τ is defined as

$$\tau = \frac{L_G}{L_E} \tag{1}$$

where L_G is the geodesic length between two connected points in the trabecular network, and L_E is the Euclidean distance. In the literature, some authors assume the Euclidean distance as the length of the straight line between these two points independently of the geometry of the phases [21]; others assume it as the distance between two parallel planes that enclose the pore structure [22] (see Fig. 1). In this work, the latter is assumed. This approach allows us to consider a thin cylindrical pore that is not perpendicular to the planes as having a tortuosity $\tau > 1$.

To estimate the tortuosity of the trabecular bone, we adapted the GR algorithm proposed in [22]. An overview of the 2-D and 3-D GR algorithm is provided in the Appendix.

Applying the 3-D GR with a six-neighbor structure element (SE_6) in the six directions for each one of the 15 samples and estimating the tortuosity by the slope of the best fit line for the points $(L_E, \langle L_G \rangle)$, we get the results presented in Table I. The tortuosity presents directional sensitivity and may differ

TABLE I
TORTUOSITY ESTIMATIONS IN EACH DIRECTION FOR THE 15 SAMPLES, BY GR WITH SE_6

Sample	τ_{+z}	τ_{-z}	τ_{+y}	τ_{-y}	τ_{+x}	τ_{-x}
254	1.2895	1.2779	1.4726	1.4569	1.6514	1.6847
255	1.2618	1.2749	1.4693	1.4556	1.6534	1.6137
256	1.2711	1.2807	1.587	1.5317	1.6582	1.6973
262	1.2574	1.2486	1.5057	1.4857	1.6496	1.5766
263	1.3159	1.312	1.4512	1.4046	1.6659	1.7408
264	1.2686	1.2722	1.4776	1.4271	1.5043	1.5046
265	1.1716	1.1668	1.4345	1.4118	1.4608	1.4664
266	1.2591	1.2500	1.4459	1.4126	1.6284	1.6075
267	1.2452	1.2478	1.4881	1.4676	1.5739	1.5183
268	1.4453	1.4403	1.5571	1.5316	1.8812	1.8237
269	1.3108	1.2853	1.6766	1.5668	2.0818	2.2224
270	1.3207	1.2792	1.6012	1.5632	1.7564	1.6771
271	1.2541	1.2384	1.5541	1.5222	1.5471	1.6465
272	1.3377	1.3026	1.5686	1.5575	1.7688	1.8355
273	1.4291	1.429	1.6344	1.5358	2.1542	2.0394

TABLE II
BV/TV AND EPC_V FOR THE 15 SAMPLES

Sample	BV/TV	EPC_V
254	0.0791	-3.413
255	0.0736	-1.520
256	0.0879	-2.745
262	0.0998	-4.075
263	0.0821	-3.015
264	0.1066	-1.458
265	0.1451	-4.910
266	0.1055	-5.130
267	0.1242	-3.879
268	0.0652	-0.337
269	0.0376	-0.261
270	0.0641	-0.816
271	0.0741	-1.909
272	0.0718	-2.037
273	0.0353	-0.375

according to the sweeping direction. In the particular case of the $\pm k, k = x, y$, and z directions, the tortuosity values differ due to the fact that the GR algorithm reconstructs a few distinct trabeculae in each sweeping direction, which is a consequence of the nonconnectedness of these trabeculae to the reconstructed ones; for instance, they can appear coming from one side ($-k$ direction) without having connectivity with those trabeculae coming from the opposite side ($+k$ direction), and also due to their shapes exhibiting more plateness or rodness in the sweeping plane direction.

2) Trabecular Volume Fraction: The trabecular volume fraction [23] is estimated by the ratio BV/TV, where BV is the trabecular bone volume estimated by counting the voxels corresponding to trabeculae and TV is the total tissue volume of the sample. Table II exhibits the trabecular volume fraction for the 15 samples.

The trabecular volume fractions were estimated considering the whole trabecular network of each sample. Nevertheless, when geodesically reconstructing the trabecular network not all trabeculae are reconstructed due to the fact that some of them are isolated or are not directly connected to the trabeculae initially swept by the plane. If we take into account only the trabeculae that are geodesically reconstructed, the trabecular volume fraction is a bit smaller than the one for the whole sample. Computing the volume fraction for the reconstructed trabecular network in each direction for all samples and the relative error to the actual trabecular volume fraction, given by

$$R_{\pm k} = \frac{\mathrm{BV/TV} - (\mathrm{BV/TV})_{\pm k}}{\mathrm{BV/TV}} \tag{2}$$

where $\pm k$ indicates the sweeping directions (x, y, z), we have noticed that the error is bounded to $0 \leq R_{\pm k} \leq 0.03$, or it has a maximum of 3%, which can actually be neglected. Therefore, in what follows, we assume the trabecular volume fraction of the whole sample.

3) Trabecular Connectivity: The network connectivity is an important topological property of the trabecular structure. The EPC [24]–[26] has been used to estimate the trabecular connectivity. In simple terms, the EPC for a collection of 3-D objects is given by $N_V - C_V$, where N_V is the number of disconnected parts (zero Betti number) and C_V is the connectivity (genus or first Betti number) of the pore space per unit volume. The EPC can be computed from a set of parallel images [27] with a small distance apart (disectors) by

$$\mathrm{EPC} = \frac{1}{2}(\sharp I - \sharp B + \sharp H) \tag{3}$$

where $\sharp I$ is the number of objects (isolated parts), $\sharp B$ is the number of tunnels (redundant connections), and $\sharp H$ is the number of enclosed cavities (holes). EPC gets smaller for higher connectivity. As the size of our samples are different from each other, we can normalize this estimation dividing the EPC values by the respective volume, obtaining the average of connections by mm^3, EPC_V, presented in Table II.

4) Young Modulus of Elasticity: The material elasticity is another important property to be analyzed, because it reflects its stiffness and resistance when subjected to load. Imposing a strain ε to the sample, it is related with the stress σ as follows:

$$\sigma = E\varepsilon \tag{4}$$

where E is the Young modulus of elasticity. Usually, σ is obtained from the sample reaction force, divided by the area which is being displaced. Rigorously, the trabecular structure is not isotropic [28]–[30]; hence E should not be a scalar, but a symmetric tensor; nevertheless, considering the complexity of modeling a porous structure, an isotropic model has been assumed [17], [31]. The results obtained were subjected to the homogenization theory to find the Young modulus of a typical trabecula. Table III exhibits the Young modulus for the three positive space directions for the 15 samples.

III. RESULTS

In the previous section, the trabecular volume fractions, tortuosities, EPCs, and Young modulus of elasticity have been estimated for the set of 15 μCT image samples.

Considering the tortuosity values in the positive and negative directions for the same space dimension (x, y, or z), one can

TABLE III
YOUNG MODULUS IN MPA UNITS FOR THE 15 SAMPLES

Sample	E_x	E_y	E_z
254	11.9968	26.3141	109.9181
255	19.9613	42.3111	125.7052
256	12.2158	7.1886	100.7650
262	35.5662	32.6686	195.1843
263	14.5422	77.4269	193.7779
264	52.5948	57.4134	201.2538
265	74.0586	70.4234	478.3804
266	100.8939	37.9518	266.8906
267	78.0658	49.2447	304.2088
268	21.3644	8.9698	33.1618
269	9.3033	0.2980	32.9391
270	52.8751	37.1958	217.9997
271	21.4250	22.6488	177.4416
272	13.6451	20.4094	119.0552
273	3.7583	15.2647	53.2031

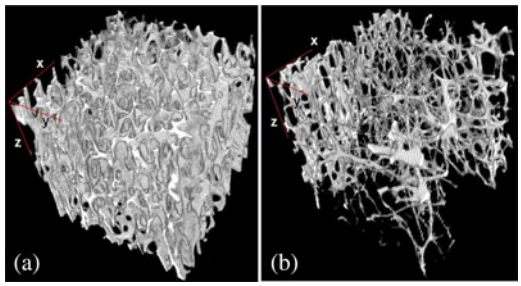

Fig. 2. (a) 3-D visualization of sample 265, with a high connectivity and E_z. (b) 3-D visualization of sample 269, with a low connectivity and E_z.

see they vary significantly according to the structure quality. This fact was treated in previous works [32], [33]. Here, we will focus in the positive directions, since the elasticity simulation was performed prioritizing them.

According to the tortuosities for each sample, we notice that the smallest values occur in the z-direction, which, taking into account the sample orientation, means the longitudinal direction of the radius. It is an indication that the trabecular network tends to get aligned in the direction where it is mostly submitted to tensile or compressive stresses [29], [34]. From Table III, the highest E also occurs in z-direction: the trabeculae alignment raises the trabecular strength and capacity to load. This result enforces our conjecture that tortuosity plays an important role to the mechanical competence of the trabecular structure and scaffold, and so it needs to be further investigated.

Looking at the 3-D visualization of sample 269 [see Fig. 2(b)] and the respective results in Tables I and II, it can be seen that it has a large cavity and low connectivity in a specific region of the trabecular network; this fact is reflected directly in the low BV/TV and high τ values, as the trabeculae that are still connected have a higher geodesic distance in consequence of large marrow cavities. The opposite occurs with better structured samples, like 265 [Fig. 2(a)]. Inasmuch, from Table III, it is possible to verify that those samples which behave like 269, with low BV/TV and connectivity, and high tortuosity values, in general, present lower values for E, as a consequence of their smaller resistance to load.

TABLE IV
CORRELATION COEFFICIENTS AND p-VALUE BETWEEN BV/TV, E_z, EPC_V, AND τ_{+z}

	BV/TV	E_z	EPC_V
E_z	0.87 (2.4E-05)	1	
EPC_V	-0.82 (1.7E-4)	-0.73 (1.8E-03)	1
τ_{+z}	-0.76 (1E-03)	-0.75 (1.2E-03)	0.71 (2.8E-03)

To corroborate this conjecture, a linear correlation analysis was performed between the four representative parameters. From Table IV, it can be seen that BV/TV has a high negative coefficient with respect to EPC_V and also with τ_{+z}. This means that the higher the volume fraction, the higher the connectivity (lower EPC_V values), and better aligned is the trabecular network (lower τ). Furthermore, the relation between BV/TV and E_z is strongly positive, which means that the more bone content, the higher will be the resistance to the load. The relationship between EPC_V and τ indicates that the better connected the trabecular network is, the higher will be the directional alignment of the structure. The negative correlation between EPC_V and E_z as well as between τ_{+z} and E_z indicates that the more connected and better aligned are the trabeculae, the stiffer will be the structure.

It is worth pointing out also the high correlation coefficients observed between E_z and τ_{+y} ($r = -0.65, p = 0.0083$) and τ_{+x} ($r = -0.72, p = 0.0026$). This indicates the importance of the horizontal ties, which are first lost when the bone structure starts to deteriorate [5].

A. Principal Component Analysis

Since high correlation coefficients were found (see Table IV), a consistent PCA [35] can be performed between the parameters BV/TV, EPC_V, τ_{+z}, and E_z. The PCA provides a mean to merge the four parameters into just a single one. In the analysis, there was a dominance of a first principal component's variance over the others (3.3 versus 0.3, 0.3, and 0.1 for PC_1 versus PC_2, PC_3, and PC_4, respectively). As the variance of PC_1 is significantly higher than the rest, the parameters $\text{BV/TV}, \text{EPC}_V$, T_{+z}, and E_z can be represented by a best fit line.

According to the previous analysis, the MCP is defined as

$$\text{MCP} = 0.52\,\text{BV/TV} - 0.49\,\text{EPC}_V + 0.51\,E_z - 0.48\,\tau_{+z} \tag{5}$$

and the values for the 15 distal radius samples are given in Fig. 3. From these results, it can be seen that sample 269 has the lowest MCP value and sample 265 has the highest value, which is in agreement with the expected. In other words, just based on the 269 sample MCP it can be inferred that this sample presents low volume fraction, low connectivity, low stiffness, and high tortuosity in the z-direction, while the MCP for sample 265 presents the opposite: high volume fraction, high connectivity, high stiffness, and low trabeculae tortuosity. To provide a visual

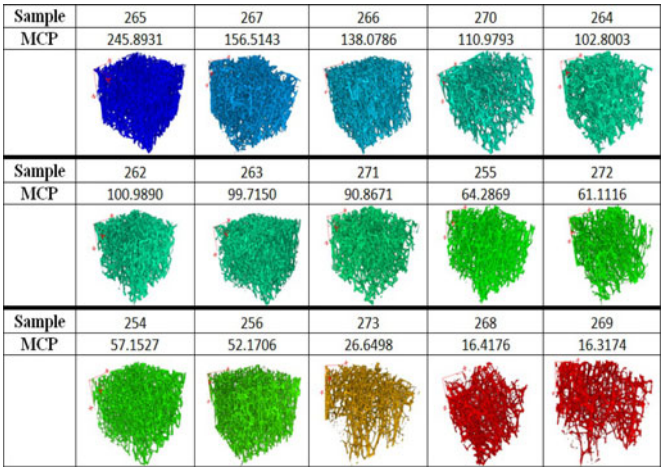

Fig. 3. MCP values and color spectrum (top-left blue to bottom-right red) of the 15 samples.

assessment to the MCP of the samples a color spectrum is shown in Fig. 3.

IV. Discussion

In this work, it has been analyzed how the trabecular volume fraction, connectivity, tortuosity, and elasticity play an important role to the mechanical competence of the structure. For that purpose, 15 distal radius trabecular bone network samples were considered in the study. To better understand the morphometrical and mechanical behavior of the samples, the four parameters were investigated, namely: trabecular volume fraction (BV/TV), EPC for the connectivity, the trabecular network tortuosity τ, and Young modulus of the elasticity E; the results are presented in Tables I–III.

With the aid of the 3-D visualization of the samples and based on these data, it can be noted that the samples with higher volume fraction and better connectivity present the smallest tortuosity values and the highest stiffness. In contrast, those samples with low volume fraction and less trabecular connectivity present the highest tortuosity values and less resistance to load. In particular, it can be observed that along the z-direction, which corresponds to the distal-proximal or longitudinal radius direction, the tortuosities are smaller compared to the x- and y-directions due to the fact that the trabecular network tends to get aligned in the direction where it is more frequently submitted to loads, in agreement to the Wolff's law [36].

As far as the authors are concerned, no previous work is available in the literature about the trabecular bone mechanical competence based on these four parameters. However, there have been some studies about the marrow cavity tortuosities by experimental ultrasound techniques. In [12], the tortuosities of the marrow cavities for five stereolithographical bone replicas were estimated using audiofrequency pulses. The replicas were from iliac crest, femoral head, calcaneus, and lumbar spine (LS2B and LS4A), and the tortuosities mean values were in the range of $1.042 \leq \langle\tau\rangle \leq 1.694$. The highest mean values of the tortuosities were for the femoral head and iliac crest and the smallest were from the lumbar spine replicas, with $\langle\tau_x\rangle = 1.042 \pm 0.017$, where the x-direction in their work corresponds to the main direction of alignment. In [37], tortuosity estimations were also done for the marrow cavities for 28 human femur specimens *in vitro*, using electrical spectroscopy, with the values in the range $1.1 \leq \tau \leq 2.8$ and a mean $\langle\tau\rangle = 1.5$.

As the tortuosity estimations done in [12] and [37] were for the pore phase (marrow cavities), using different methodologies and different trabecular sites, it was not possible to perform a straightforward comparison between their results and ours. Nevertheless, to get somehow closer to their results, we have also estimated the tortuosities of the marrow cavities of our samples, that is, to the complement of the trabecular network, and the results for the distal radius samples were $\langle\tau_z\rangle = 1.022 \pm 0.007$, $\langle\tau_y\rangle = 1.033 \pm 0.017$, and $\langle\tau_x\rangle = 1.046 \pm 0.018$. We can see that the marrow cavity tortuosities of the distal radius bone are comparable to the lumbar spine, particularly in the direction of main alignment.

The PCA performed for the parameters (BV/TV, EPC_V, E_z, and τ_{+z}) has shown that the first principal component can suitably simultaneously describe the corresponding characteristics of the trabecular bone network structure. Defining the main PC as the MCP, it provides a simple and direct way to characterize and analyze the mechanical competence for a group of trabecular bone samples. The MCP color spectrum of the samples provides a visual quality level assessment to the trabecular bone structural fragility.

The study has some limitations that must be addressed. First, the FE analysis is performed in the linear domain and it is known that in bone fracture there is an important progression of the structure toward collapse. Future advances in computation will permit the nonlinear analysis of the FE models with reduced computational burden. Also, as the MCP is first introduced in this manuscript for a small group of *ex vivo* samples, normality results and ranges of MCP in a healthy population are not yet available. It should be mentioned that although we do not have experimental testing of the specimens, the methodology used in this manuscript was validated by the authors in polymer scaffolds [38]. The study will be continued by analyzing the results of MCP *in vivo*, from high spatial resolution (MRI, HR-pQCT), in order to analyze the relationship of the parameter with age and sex.

V. Conclusion

In this study, the tortuosity of the trabecular network has been introduced as a structural parameter with high influence in establishing the directional strength of the structure. A novel MCP, unifying tortuosity, connectivity, morphology, and elasticity information, has been proposed for a more direct assessment and grading of the trabecular bone fragility in osteoporotic patients. The analyses have been performed based on μCT images of *ex vivo* distal radius samples. Clearly, μCT is not allowed for *in vivo* subjects due to high radiation; therefore, a study is in progress to estimate the MCP based on MRI and HR-pQCT, as well. This study in large populations *in vivo* will help to improve the bone microarchitecture quality characterization supporting health programs for osteoporosis prevention and treatment.

APPENDIX

GEODESIC RECONSTRUCTION

In a recent paper, Gommes *et al.* [22] proposed an algorithm to estimate the tortuosity of a pore network based on GR of the image. The technique reconstructs the pore image pixel by pixel, growing along its main direction. In this way, to geodesically reconstruct a pore, the computational cost will depend on how much tortuous the pore is; as more tortuous it is, more reconstructions are necessary to recover it. The algorithm of GR can be applied to 2-D or 3-D binary images.

According to [22], if the distance between two points in a pore is only few times the average pore size, the ratio L_G/L_E might not be so relevant for the transport properties of the material. Therefore, a more suitable definition for the geometric tortuosity would be

$$\tau = \lim_{L_G \to \infty} \frac{L_G}{L_E}. \tag{6}$$

From this definition, for very large values of L_G the locus of all points at a given Euclidean distance L_E from another point is approximately at a plane surface. In this regard, we may consider the tortuosity measured by comparing the geodesic and Euclidean distances between planes rather than between points. This approach is useful for the estimation of tortuosity on image space. Defining $\rho(L_E, L_G)$ as the joint distribution for the Euclidean and geodesic distances, the average value of L_G corresponding to a specific value of L_E is given by

$$\langle L_G \rangle = \frac{\int_0^\infty \rho(L_E, L_G) L_G dL_G}{\int_0^\infty \rho(L_E, L_G) dL_G}. \tag{7}$$

From (7), it is possible to plot the set of points $(L_E, \langle L_G \rangle)$ for the trabecular bone network and estimate the tortuosity as the slope of the best fit line for these points (see Fig. 4).

A. Geodesic Reconstruction Algorithm

The GR algorithm proposed in [22] can be applied to 2-D or 3-D images. Here, we briefly describe the GR for binary images.

1) 2-D GR Algorithm: For 2-D binary images a four-neighbor or an eight-neighbor structure element, SE_4 or SE_8, respectively, can be considered. The SE_4 does not take into account the pixels that are on the diagonal of the central pixel, though this increases the computational cost of the algorithm to reconstruct the trabecular tortuosity. Nevertheless, the use of SE_4 is justified as the trabecular connectivity through a vertex represents a very weak connectivity.

The reconstruction algorithm works as follows: let us consider the trabeculae as white pixels and their complement (e.g., marrow) as gray pixels to ease the visualization. Let I be the initial 2-D image. Assuming a sweep line at pixels column $x = 0$ and sweeping toward the positive x-direction, the algorithm starts putting the first column with white pixels (r_0); the image r_0 is dilated using SE_4 ($\oplus SE_4$) resulting an image d_1. The image d_1 is then intersected with the initial image I, obtaining the image r_1. This process is repeated now dilating r_1 with SE_4 and so on until the dilated image gives a null intersection with the initial image I. The intersection operation $\cap$ is the familiar operation

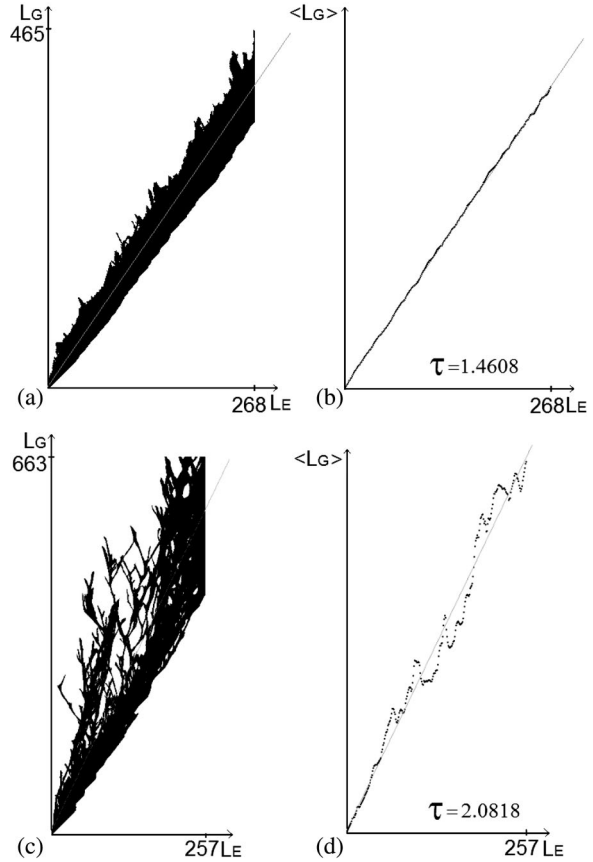

Fig. 4. Plot of distance distributions of samples (a) 265 and (c) 269; graph of the points $(L_E, \langle L_G \rangle)$, with tortuosity value for the trabecular samples (b) 265 and (d) 269. The plots were for the positive x-direction in both cases.

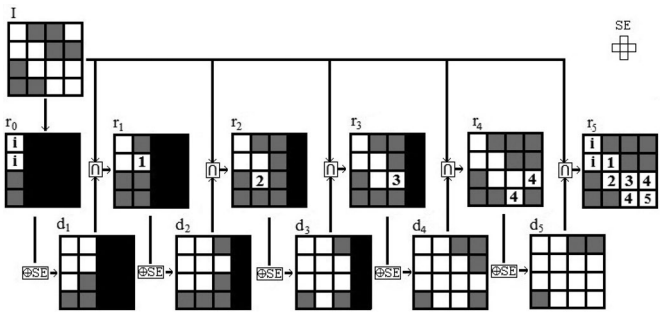

Fig. 5. Illustration of the GR algorithm applied to a 2-D image with 4×4 pixels and SE_4. Notice that the isolated pixel on the upper right corner is eliminated during the procedure. The reconstruction number is indicated inside the pixels.

on binary images, that is, a pixel assumes the value 1 (white) if and only if in both images they have the value 1. In Fig. 5, the GR algorithm is illustrated step-by-step for a square image I with 16 pixels.

2) 3-D GR Algorithm: For 3-D images the GR algorithm follows the same steps as for 2D, just taking now a sweep plane instead of a sweep line, the initial column is now substituted by an initial sweeping plane that can sweep the trabecular network in the x-, y-, or z-directions, and either a 6-, 18-, or 26-neighbor structure element (SE_6, SE_{18}, or SE_{26}). By similar argument as

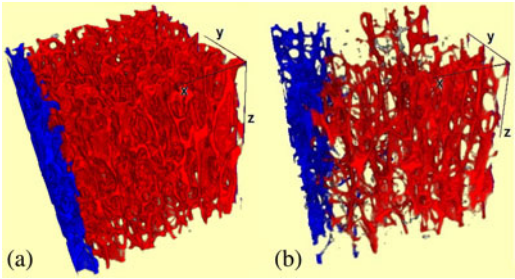

Fig. 6. In red (or gray), the geodesically reconstructed trabecular network with SE_6 up to the 240th GR. In blue (or black) the trabeculae that were not yet reconstructed and the white ones are those isolated. (a) sample 265, direction $+x$; (b) sample 269, direction $+x$.

for 2-D binary images, the SE_{18} would lead to trabecular connectivity through voxel edges, while the SE_{26} would let connectivity through voxel vertex as well. Therefore, we consider in this paper GR based on SE_6.

Fig. 4 presents the plot of the distribution $\rho(L_E, L_G)$ and the graph of $(L_E, \langle L_G \rangle)$ from a trabecular bone sample. The tortuosity can then be estimated as the slope of the best fit line. Fig. 6 exhibits a 3-D GR with SE_6 for a trabecular network. The trabeculae that were already reconstructed up to the 240th RG are shown in red; the trabeculae after the 240th GR are shown in blue and the white ones correspond to the trabeculae that are isolated.

ACKNOWLEDGMENT

W. L. Roque would like to thank Dr. Z. Tabor for several discussions.

REFERENCES

[1] R. Burge, B. Dawson-Hughes, D. H. Solomon, J. B. Wong, A. Kin, and A. Tosteson, "Incidence and economic burden of osteoporosis-related fractures in the United States: 2005–2025," *J. Bone Miner. Res.*, vol. 22, no. 3, pp. 465–475, 2007.

[2] D. V. Araújo, J. H. Oliveira, and O. L. Bracco, "Custo da fratura osteoporótica de fêmur no sistema suplementar de saúde brasileiro," *Arq. Bras. Endocrinol. Metab.*, vol. 49, no. 6, pp. 897–901, 2005.

[3] S. Tassani, F. Demenegas, and G. K. Matsopoulos, "Local analysis of trabecular bone fracture," in *Proc. IEEE 33rd Annu. Int. Conf. Eng. Med. Biol. Soc.*, Aug./Sep. 2011, pp. 7454–7457.

[4] J. Homminga, B. R. Mccreadie, H. Weinans, and R. Huiskes, "The dependence of the elastic properties of osteoporotic cancellous bone on volume fraction and fabric," *J. Biomech.*, vol. 36, no. 10, pp. 1461–1467, 2003.

[5] L. D. Carbonare, M. T. Valenti, F. Bertoldo, M. Zanatta, S. Zenari, G. Realdi, V. L. Cascio, and S. Giannini, "Bone microarchitecture evaluated by histomorphometry," *Micron*, vol. 36, no. 7–8, pp. 609–616, 2005.

[6] A. P. Accardo, I. Strolka, R. Toffanin, and F. Vittur, "Medical imaging analysis of the three dimensional (3D) architecture of trabecular bone: Techniques and their applications," in *Medical Imaging Systems Technology—Methods in General Anatomy*, C. T. Leondes, Ed. Singapore: World Scientific, 2005.

[7] M. Dierolf, A. Menzel, P. Thibault, P. Schneider, C. M. Kewish, R. Wepf, O. Bunk, and F. Pfeifer, "Ptychographic X-ray computed tomography at the nanoscale," *Nature*, vol. 467, no. 7314, pp. 436–439, 2010.

[8] W. L. Roque, K. Arcaro, and Z. Tabor, "An investigation of the mechanical competence of the trabecular bone," *Mecânica Computacional*, vol. XXIX, E. Dvorkin, M. Goldschmit, and M. Storti, Eds. Buenos Aires, Argentina: AMCA, pp. 2001–2009, 2010.

[9] P. K. Saha, Y. Xu, H. Duan, A. Heiner, and G. Liang, "Volumetric topological analysis: A novel approach for trabecular bone classification on the continuum between plates and rods," *IEEE Trans. Med. Imag.*, vol. 29, no. 11, pp. 1821–1838, Nov. 2010.

[10] K. J. L. Burg, S. Porter, and J. F. Kellam, "Biomaterial developments for bone tissue engineering," *Biomaterials*, vol. 21, no. 23, pp. 2347–2359, 2000.

[11] M. B. Clennell, "Tortuosity: A guide through the maze," in *Developments in Petrophysics*, vol. 122. London, U.K.: Geological Society, pp. 299–344, 1997

[12] K. Attenborough, H.-C. Shin, M. J. Fagan, and C. M. Langton, "Measurements of tortuosity in stereolithographical bone replicas using audiofrequency pulses (L)," *J. Acoust. Soc. Amer.*, vol. 118, no. 5, pp. 2779–2782, 2005.

[13] E. R. Hughes, T. G. Leighton, and P. R. White, "Investigation of an anisotropic tortuosity in a biot model of ultrasonic propagation in cancellous bone," *J. Acoust. Soc. Amer.*, vol. 121, no. 1, pp. 568–574, 2007.

[14] H. Aygun, K. Attenborough, M. Postema, W. Lauriks, and C. M. Langton, "Predictions of angle dependent tortuosity and elasticity effects on sound propagation in cancellous bone," *J. Acoust. Soc. Amer.*, vol. 126, no. 6, pp. 3286–3290, 2009.

[15] A. Laib, O. Beuf, A. Issever, D. C. Newitt, and S. Majumdar, "Direct measures of trabecular bone architecture from MR images," *Adv. Exper. Med. Biol.*, vol. 496, pp. 37–46, 2001.

[16] N. Otsu, "A threshold selection method from gray-level histograms," *IEEE Trans. Syst. Man Cybern.*, vol. 9, no. 1, pp. 62–66, Jan. 1979.

[17] A. Alberich-Bayarri, L. Marti-Bonmati, M. A. Perez, J. J. Lerma, and D. Moratal, "Finite element modeling for a morphometric and mechanical characterization of trabecular bone from high resolution magnetic resonance imaging," in *Finite Element Analysis*, D. Moratal, Ed. Rijeka, Croatia: Scyio Publishing, 2010, pp. 195–208.

[18] A. Alberich-Bayarri, L. Marti-Bonmati, R. Sanz-Requena, E. Belloch, and D. Moratal, "In vivo trabecular bone morphological and mechanical relationship using high resolution 3T MRI," *Amer. J. Roentgenol.*, vol. 191, no. 3, pp. 721–726, 2008.

[19] Y. C. Fung, *Biomechanics: Mechanical Properties of Living Tissues*, 2nd ed. New York: Springer-Verlag, 1993.

[20] S. J. Hollister, D. P. Fyhrie, K. J. Jepsen, and S. A. Goldstein, "Application of homogenization theory to the study of trabecular bone mechanics," *J. Biomech.*, vol. 24, no. 9, pp. 825–839, 1991.

[21] Y. S. Wu, L. J. van Vliet, H. W. Frijlink, and K. V. Maarschalk, "The determination of relative path length as a measure for tortuosity in compacts using image analysis," *Eur. J. Pharm. Sci.*, vol. 28, no. 5, pp. 433–440, 2006.

[22] C. J. Gommes, A.-J. Bons, S. Blacher, J. H. Dunsmuir, and A. H. Tsou, "Practical methods for measuring the tortuosity of porous materials from binary or gray-tone tomographic reconstructions," *AIChE J.*, vol. 55, no. 8, pp. 2000–2012, 2009.

[23] D. Chappard, E. Legrand, C. Pascaretti, M. F. Basl, and M. Audran, "Comparison of eight histomorphometric methods for measuring trabecular bone architecture by image analysis on histological sections," *Microsc. Res. Tech.*, vol. 45, nos. 4–5, pp. 303–312, 1999.

[24] H. J. Vogel and A. Kretzschmar, "Topological characterization of pore space in soil—Sample preparation and digital image-processing," *Geoderma*, vol. 73, nos. 1–2, pp. 23–38, 1996.

[25] H. J. G. Gundersen, R. W. Boyce, J. R. Nyengaard, and A. Odgaard, "The connEulor: Unbiased estimation of the connectivity using physical disectors under projection," *Bone*, vol. 14, no. 3, pp. 217–222, 1993.

[26] N. Roberts, M. Reed, and G. Nesbitt, "Estimation of the connectivity of a synthetic porous medium," *J. Microsc.*, vol. 187, no. 2, pp. 110–118, 1997.

[27] W. L. Roque, A. C. A. Souza, and D. X. Barbieri, "The euler-poincaré characteristic applied to identify low bone density from vertebral tomographic images," *Revista Brasileira Reumatol.*, vol. 49, no. 2, pp. 140–152, 2009.

[28] Z. Tabor and E. Rokita, "Quantifying anisotropy of trabecular bone from gray-level images," *Bone*, vol. 40, no. 4, pp. 966–972, 2007.

[29] Z. Tabor, "On the equivalence of two methods of determining fabric tensor," *Med. Eng. Phys.*, vol. 31, no. 10, pp. 1313–1322, 2009.

[30] R. Hambli, A. Bettamer, and S. Allaoui, "Finite element prediction of proximal femur fracture pattern based on orthotropic behaviour law coupled to quasi-brittle damage," *Med. Eng. Phys.*, vol. 34, no. 2, pp. 202–210, 2012.

[31] W. B. Edwards and K. L. Troy, "Finite element prediction of surface strain and fracture strength at the distal radius," *Med. Eng. Phys.*, vol. 34, no. 3, pp. 290–298, 2012.

[32] W. L. Roque, K. Arcaro, and I. Freytag, "Tortuosidade da rede do osso trabecular a partir da reconstruo geodésica de imagens binárias tridimensionais," in *Proc. Anais do XI Workshop de Inf. Méd.*, 2011, pp. 1708–1717.
[33] W. L. Roque, K. Arcaro, and R. B. Lanfredi, "Tortuosidade e conectividade da rede trabecular do rádio distal a partir de imagens microtomográficas," *Rev. Bras. Eng. Bio.*, vol. 28, pp. 116–123, 2012.
[34] H. Gong, D. Zhu, J. Gao, L. Lv, and X. Zhang, "An adaptation model for trabecular bone at different mechanical levels," *Biomed. Eng. Online*, vol. 9, no. 32, pp. 1–17, 2010.
[35] I. T. Jolliffe, *Principal Component Analysis*. New York: Springer-Verlag, 2002.
[36] J. Wolff, *The Law of Bone Remodeling.* Berlin, Germany: Springer-Verlag, 1986 (translation of the German 1892 edition).
[37] M. Pakula, F. Padilla, P. Laugier, and M. Kaczmarek, "Application of biots theory to ultrasonic characterization of human cancellous bones: Determination of structural, material and mechanical properties," *J. Acoust. Soc. Amer.*, vol. 123, no. 4, pp. 2415–2423, 2008.
[38] A. Alberich-Bayarri, D. Moratal, J. L. Escobar, J. C. Rodrguez, A. Valls, L. Marti-Bonmati, J. Ms, J. F. Mano, M. Monlen Pradas, J. L. Gmez, and M. Salmern, "Micro-computed tomography and micro-finite element modelling for evaluating polymer scaffolds architecture and their mechanical properties," *J. Biomed. Mater. Res. Part B. Appl. Biomater.*, vol. 91B, pp. 191–202, 2009.

Authors' photographs and biographies not available at the time of publication.